J. Fluid Mech. (2011), *vol.* 689, *pp.* 203–220.
doi:10.1017/jfm.2011.411

Air-induced inverse Chladni patterns

Henk Jan van Gerner[1,2], Ko van der Weele[3], Martin A. van der Hoef[1,4] and Devaraj van der Meer[1]†

[1] Faculty of Science and Technology, University of Twente, P.O. Box 217, 7500 AE Enschede, The Netherlands

[2] National Aerospace Laboratory, P.O. Box 153, 8300 AD Emmeloord, The Netherlands

[3] Department of Mathematics, University of Patras, 26500 Patras, Greece

[4] Department of Chemical Engineering and Chemistry, Eindhoven University of Technology, P.O. Box 513, 5600 MB Eindhoven, The Netherlands

(Received 17 December 2009; revised 27 March 2011; accepted 16 September 2011)

When very light particles are sprinkled on a resonating horizontal plate, inverse Chladni patterns are formed. Instead of going to the nodal lines of the plate, where they would form a standard Chladni pattern, the particles are dragged to the antinodes by the air currents induced by the vibration of the plate. Here we present a detailed picture of the mechanism using numerical simulations involving both the particles and the air. Surprisingly, the time-averaged Eulerian velocity, commonly used in these type of problems, does not explain the motion of the particles: it even has the opposite direction, towards the nodal lines. The key to the inverse Chladni patterning is found in the averaged velocity of a tracer particle moving along with the air: this Lagrangian velocity, averaged over a vibration cycle, is directed toward the antinodes. The Chladni plate thus provides a unique example of a system in which the Eulerian and Lagrangian velocities point in opposite directions.

Key words: granular media, particle/fluid flow

1. Introduction

A classic way of visualizing two-dimensional standing waves is by sprinkling coarse particles (such as sand grains or salt) on a horizontal plate and bringing it into resonance using, e.g., a violin bow. The particles will move to the nodal lines, giving rise to the well-known Chladni patterns, a standard high school demonstration experiment (Chladni 1802, 1809; Stöckmann 2006, 2007). The technique was developed by Ernst Chladni in 1787 who actually became quite famous with it and toured extensively throughout Europe. In 1809, he was invited to perform his experiment before Napoleon, who was so pleased with it, that he awarded Chladni 6000 francs. Napoleon also promised 3000 francs to anyone who could provide the mathematical theory for the sound figures. This sum was awarded to Sophie Germain in 1816 (Stöckmann 2007), who described the eigenmodes of a square plate (with boundary conditions liberally different from those in Chladni's experiment, just like in

† Email address for correspondence: d.vandermeer@utwente.nl

the present work) and identified the nodal lines as the regions towards which the sand particles would move.

Much less known, and not mentioned in Germain's account, is that very light particles will move to the antinodes, although also this was already noted by Chladni himself, who observed that tiny hair shavings from his violin bow were carried to the antinodes. In 1831, the effect was studied more systematically by Faraday with the use of lycopodium powder (Faraday 1831). He and others showed that the inverse Chladni patterning of fine particles is due to air currents induced by the vibrating plate (Faraday 1831; Waller 1955; Dorrestijn *et al.* 2007), dragging along the fine particles to the antinodes. The mathematical explanation for these air currents was first provided by Lord Rayleigh in 1884 (Rayleigh 1884, 1894) and the phenomenon is therefore often referred to as Rayleigh streaming or, since much of the early research was concerned with air currents induced by sound waves, acoustic streaming. This last term, however, is less appropriate for the particular streaming that causes the inverse Chladni patterns since here the compressibility of the air plays no significant role. In this paper we use the term 'steady streaming' (Riley 2001). It should be noted that the inverse Chladni patterns discussed here are also distinctly different from the granular streaming patterns described by Savage (1988), since those arise from dissipation in the interior of the granular material.

Despite all of the experimental and theoretical investigations it has instigated, a detailed picture of the intricate dynamics of the air and the particles in Chladni's classic experiment is still lacking. The purpose of the present paper is to provide exactly such a picture. We do this by means of direct numerical simulations (introduced in § 2) that allow us to follow the air currents and all particle trajectories during an entire vibration cycle, which is hard to accomplish, if not impossible, in experiments or in a purely analytical approach. The result is a particularly clear illustration of the physical mechanisms at work on the Chladni plate. Among other things, in § 3 we show that the Lagrangian velocity field (the velocity of tracer particles following the flow of the air) is much more relevant for explaining the inverse Chladni patterns than the more common Eulerian velocity field (as measured by probes at fixed points in space). In fact, it turns out that the two velocities point in opposite directions, which makes the Chladni plate a prototypical example for demonstrating the difference between Lagrangian and Eulerian streaming. In § 4 we put the above results (pertaining to the classic experiment of Chladni and Faraday) in a broader context by discussing the effects of varying the three dimensionless parameters that govern the system. Here, among other things, we use our simulation to follow the transition from inverse to regular Chladni patterning by gradually increasing the density of the particles. Finally, § 5 contains our main conclusion.

The paper is accompanied by two appendices in which we discuss (A) the mathematical modelling of streaming and (B) the difference between the steady streaming discussed in the present paper and the phenomenon of acoustic streaming.

2. Numerical model

The simulated system consists of a flexible rectangular plate (40×40 mm^2) on which 80 000 beads with a diameter $d = 0.075$ mm are uniformly distributed. The particles have a density ρ which constitutes our main control parameter in this study. The plate is flexible and pinned along its outer rim. We excite the 2×2 natural mode depicted in figure 1. Ignoring the additional bending of the plate due to gravity, the

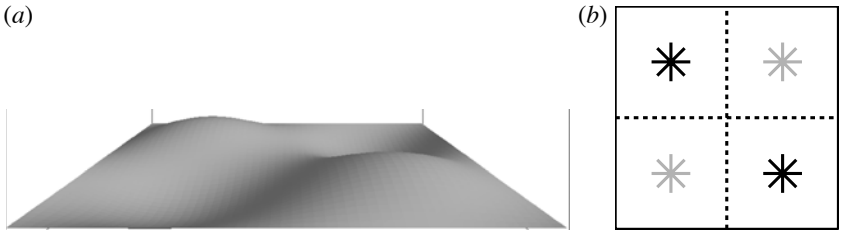

FIGURE 1. (*a*) Side view of the simulated set-up: a flexible plate of dimensions 40×40 mm^2 resonating in its 2×2 mode. On this plate we can sprinkle 80 000 particles (see figures 3 and 9) of variable density. Also included in the simulation is the air above the plate, which is set into motion by the plate's vibration (see figures 2, 5–8); the system is covered by an immobile top lid at a height $z = 2$ mm above the equilibrium position of the plate. The vertical deflection of the plate, described by (2.1) with amplitude $a = 0.075$ mm, is exaggerated 40 times for clarity. The plate is depicted at time $t = 0$ s (mod T), where $T = 0.005$ s is the period of vibration. (*b*) Top view of the set-up: the dashed lines, together with the edges of the plate, denote the nodal lines of the 2×2 mode; the asterisks indicate the position of the antinodes.

vertical deflection at any point (x, y) is then given by

$$z(x, y, t) = -a \sin \frac{2\pi x}{L} \sin \frac{2\pi y}{L} \cos(\omega t), \tag{2.1}$$

where $\omega = 2\pi f = 2\pi\, 200\ \mathrm{s}^{-1}$ is the natural frequency of the particular eigenmode of the plate, $a = 0.075$ mm the amplitude of the vibration (corresponding to a dimensionless acceleration $\Gamma = a\omega^2/g = 12.1$) and $L = 40$ mm determines the size of the plate. At a height $H = 2$ mm above the flexible plate, the system is covered by a rigid lid. The height H (2 mm) is chosen such that it is one order of magnitude larger than the thickness of the boundary layer $\delta \approx \sqrt{2\nu/\omega} = 0.17$ mm, with $\nu = 1.52 \times 10^{-5}$ m^2 s^{-1} the kinematic viscosity of air (i.e. the dimensionless Womersley number $\alpha = H\sqrt{\omega/2\nu}$ is of order 10). This is sufficiently large to not affect the streaming which takes place within and just above the boundary layer.

For our simulation we use the coupled granular dynamics (GD) – computational fluid dynamics (CFD) code described in van der Hoef *et al.* (2006, 2008), in which the oscillating rectangular plate is implemented as a time-dependent solid surface, impermeable for gas. The GD code calculates the particle trajectories from Newton's law, with the particle–particle interactions being given by a three-dimensional soft sphere collision model including tangential friction. This model uses a Hookean spring-dashpot model in the normal and tangential direction with the dissipation set by the normal (e_n) and tangential (e_t) restitution coefficients. If the ratio of the tangential and normal forces exceeds the static friction coefficient μ, the contact will become sliding with dissipation set by a dynamic friction coefficient which is taken to be equal to the static friction coefficient. In our simulations we have taken values that are typical for silica beads: $e_n = 0.90$, $e_t = 0.33$ and $\mu = 0.20$. The results presented in this paper only mildly depend on the precise values taken for the above parameters; especially where we use particles with a density close to that of lycopodium powder, the dynamics is almost exclusively dominated by the particle–air interaction. The CFD code evaluates the full Navier–Stokes equations by a finite difference method on a fixed, rectangular grid (Deen, van Sint-Annaland & Kuipers 2004). There is a full two-way coupling with the GD part of the code, i.e. the reaction from the drag and

pressure forces on the solid particles is included in the momentum equation for the gas phase. This is done through drag relations which depend on the cell-averaged local porosity of the granular material, based on the Ergun and Wen-Yu relations (Beetstra, van der Hoef & Kuipers 2007). For the interaction between the vibrating plate and the gas phase we use the immersed boundary method (Peskin 2002; Uhlmann 2005), especially adapted to the case of the resonating surface. In this method, the plate is randomly covered with marker points with a surface density of the order of a few points per δl^2, where δl is the grid size of the CFD model. Each of these marker points exerts a force on the fluid, and the corresponding force density is included in the hydrodynamics equations of the gas phase, and thus also included the CFD scheme. The magnitude of this force can be tuned such that the gas-phase velocity vanishes at the location of the marker point, thereby modelling 'no-slip' boundary conditions (van Gerner 2009). For the granular particles the plate is treated as a moving solid wall with which the particles collide, using the same three-dimensional soft sphere collision model and the same collision parameters as for the particle–particle interactions. A more detailed account of the simulation method can be found in the supplementary material (available at journals.cambridge.org/flm).

The simulated system is divided in 60 CFD cells along each side of the plate and 110 cells in the vertical direction in order to accurately capture the boundary layer above the plate. The time step used for the flow solver is 5×10^{-5} s, so that there are 100 time steps per vibration cycle. Since the particles used in the simulation only have a small influence on the gas flow above the vibrating plate (owing to the low particle volume fraction) we use one-way coupling, i.e. the flow field is calculated for one vibration cycle (without particles present) and subsequently used for all vibration cycles to act upon the particles. With our numerical code it would also be possible to calculate the flow field during all vibration cycles and include the two-way interaction with the particles. However, this would lead to extremely long CPU times and the results would be practically identical.

The flow field of the air above the flexible plate at time $t = 0.25T$ (with $T = 0.005$ s^{-1} the vibration period) is shown in figure 2. Note that a similar velocity profile is obtained at $t = 0.75T$, with the signs of u_x and u_y (the horizontal components of the air velocity) reversed, i.e. the air moves to-and-fro between the antinodes. At the vertical walls, periodic boundary conditions are used.

The response of a particle to the vibrating plate and the induced air flow is determined by the ratio of the forces it experiences from drag and gravity. The drag force on a particle can be approximated by Stokes' law:

$$\boldsymbol{F}_{drag} = 3\pi\mu_g d(\boldsymbol{u} - \boldsymbol{v}), \tag{2.2}$$

where μ_g is the dynamic gas viscosity, $\boldsymbol{u}$ is the local flow velocity of the gas phase and $\boldsymbol{v}$ is the velocity of the particle.

The use of Stokes' law asks for some justification. The hydrodynamic interaction with the surrounding particles (Ergun 1954) can be neglected because of the low particle concentration, while the history forces (Maxey & Riley 1983) can be neglected since $d/\sqrt{\nu/\omega} < 1$, with $d = 0.075$ mm, $\nu = 1.52 \times 10^{-5}$ m^2 s^{-1} the kinematic viscosity of air (at room temperature and atmospheric pressure) and $\omega = 1257$ s^{-1}. The Reynolds number can be estimated as $Re = Ud/\nu < a\omega d/\nu \approx 0.5$, justifying the use of Stokes' law. Finally, the proximity of the vibrating plate is known to modify Stokes' law with a multiplicative function of the ratio of the particle radius and the distance to the wall (Brenner 1961; Goldman, Cox & Brenner 1967). Close to the plate this leads

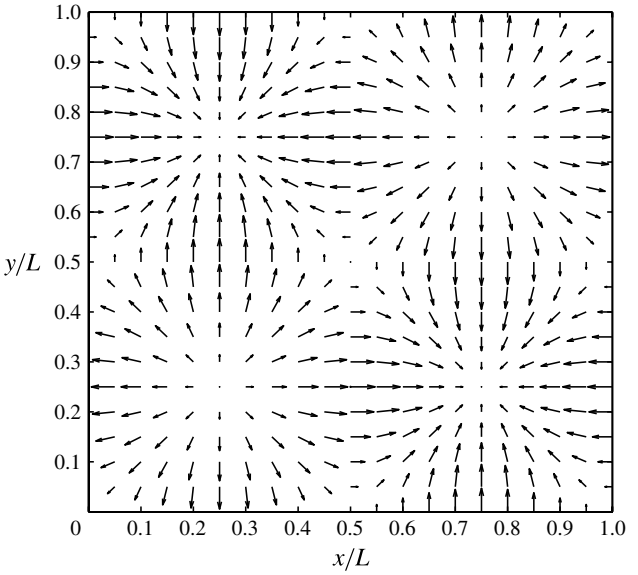

FIGURE 2. Instantaneous horizontal flow field of the air, in the absence of particles, over the resonating plate at $t = 0.25T$, when the vertical deflection given by (2.1) is momentarily zero everywhere. The depicted field has been calculated at a height $z = 0.5H$, midway between the plate and the cover, but the velocity field looks qualitatively the same also at other heights (cf. figure 5).

to small but detectable corrections to Stokes' formula, which are not considered here, since they are not expected to change our results qualitatively.

Using Stokes' law, the ratio of the (typical) drag force and gravity on a particle is

$$B = \frac{|\boldsymbol{F}_{drag}|}{|\boldsymbol{F}_g|} = \frac{3\pi\mu_g d|\boldsymbol{u} - \boldsymbol{v}|}{\rho\pi g d^3/6} \approx \frac{18\mu_g a\omega}{\rho g d^2} = \frac{\tau_g}{\tau_r}, \tag{2.3}$$

where $\tau_g = a\omega/g$ is proportional to the typical time span between two consecutive collisions with the vibrating plate and $\tau_r = \rho d^2/(18\mu_g)$ is the particle response time in the induced flow (Elghobashi 1994).

When a simulation is carried out with high-density particles (gold beads, with $\rho = 20\,000$ kg m^{-3}), the ratio B is around 0.03, i.e. the motion of the particles is governed by the Newtonian forces. Owing to the oscillations of the plate, the particles start to bounce and the successive bounces tend (on average) to increase their kinetic energy. Only at the nodal lines the plate has a zero velocity and the collisions with the plate and other particles reduce the kinetic energy of the particles. As a result, starting with all 80 000 particles distributed uniformly over the plate, within a few seconds most of them have accumulated at the nodal lines, forming a standard Chladni pattern (see figure 3*a*).

We now reduce the density of the particles to 20 kg m^{-3} while keeping the diameter constant, resulting in a typical drag force that is almost thirty times larger than the gravitational force on a particle, i.e. $B \approx 30$. This value is approximately the same as for lycopodium powder ($\rho = 460$ kg m^{-3}, diameter $d \approx 0.016$ mm (Banerjee & Law 1998)), which was used by Faraday in his experiments (Faraday 1831). As can be seen in figure 3(*b*), these light particles move to the antinodes and form an inverse Chladni pattern.

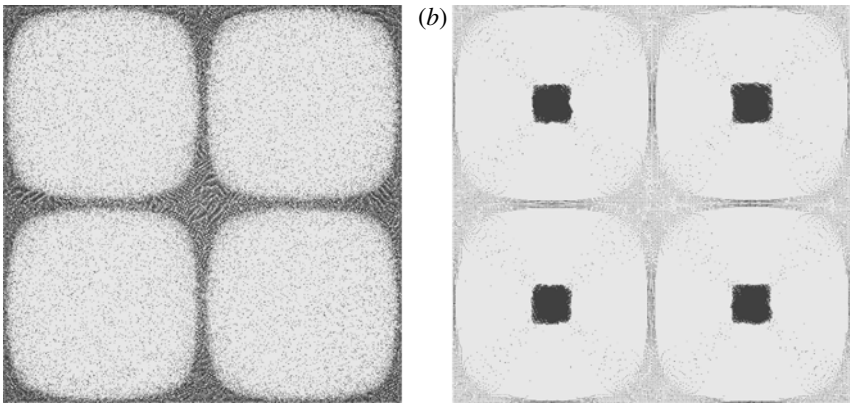

FIGURE 3. (*a*) Top view of the resonating plate of figures 1 and 2, sprinkled with 80 000 heavy particles ($\rho = 20\,000$ kg m^{-3}, diameter $d = 0.075$ mm). After a few seconds most particles have collected at the nodal lines, forming a classic Chladni pattern. (*b*) The same plate with very light particles ($\rho = 20$ kg m^{-3} and $d = 0.075$ mm). Owing to the presence of air, the particles now migrate to the antinodes and after ∼4 s an inverse Chladni pattern has formed. Movies of the formation of regular and inverse Chladni patterns can be found in the online supplementary material.

Bouncing plays no appreciable role this time, since the motion of the particles is dominated by the Stokesian forces. We further note that the particle response time $\tau_r = \rho d^2/(18\mu_g)$ (Elghobashi 1994) is $\sim 0.07T$ (with T the vibration period), so the particles are to a large extent able to follow the motion of the gas. Evidently then, the physical reason for the inverse Chladni patterning must be that the to-and-fro motion of the gas averaged over one cycle is non-zero. This counterintuitive fact is explored in the next section.

At this point it is good to note that the formation of regular and inverse Chladni patterns is not restricted to the 2×2 mode, nor to the particular plate that is used. By way of example, figure 4 shows a plate that is pinned in the middle, resonating in its second, third and fifth mode, respectively. The top row are the regular Chladni patterns formed with heavy particles; the bottom row shows the corresponding inverse Chladni patterns formed with light particles. It is only for reasons of clarity that in this paper we focus on a plate pinned at its outer rim and resonating in its 2×2 mode.

3. Steady streaming: Eulerian versus Lagrangian velocity

It is a curious but well-known fact that geometries that move sinusoidally may generate a flow field that is not simply sinusoidal: in addition to (and as a result of) the to-and-fro motion of the gas, there is a steady directed streaming near the surface of vibrating boundaries (Rayleigh 1884, 1894; Nyborg 1953; Lighthill 1978; Riley 2001). A short mathematical description of steady streaming is given in appendix A, in which it is shown how the streaming velocity is linked to the square of the instantaneous velocity, integrated over one cycle. Here, we address the physical origin of the streaming flow.

In figure 5 we show the velocity component $u_x(x, y, z, t)$ of the air above two representative points $\{x, y\}$ on the plate (indicated in the insets), as a function of z at four consecutive moments t during the vibration cycle.

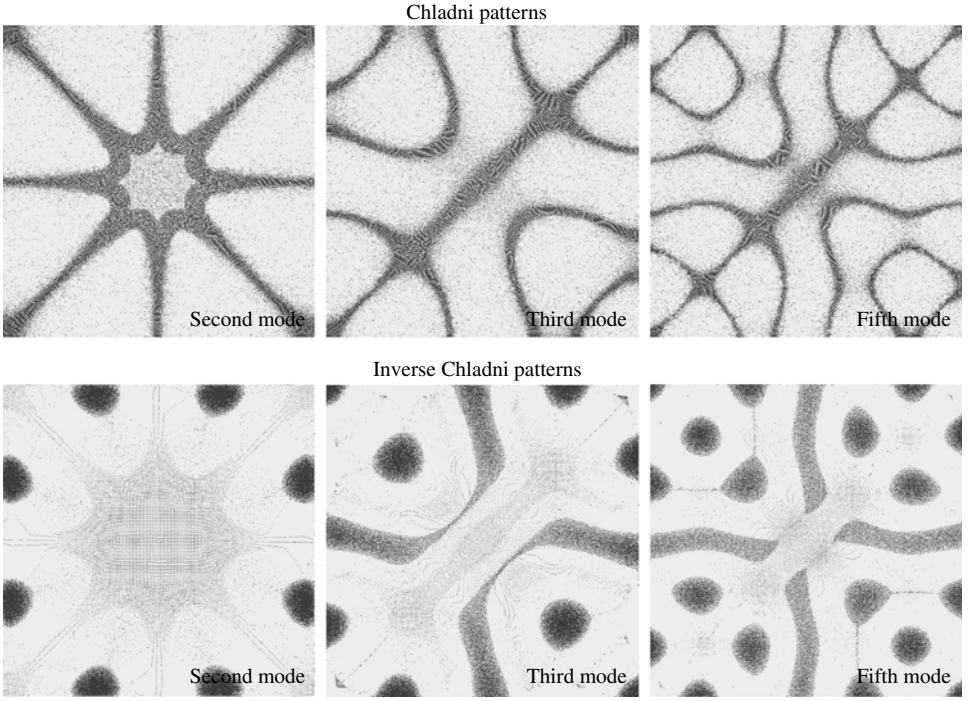

FIGURE 4. Regular and inverse Chladni patterns formed on a flexible plate pinned in the middle and excited at different eigenfrequencies. The top row shows the regular Chladni patterns obtained with heavy particles ($\rho = 20\,000$ kg m^{-3}, $d = 0.075$ mm), while the bottom row shows the corresponding inverse patterns that are obtained when light particles are used ($\rho = 20$ kg m^{-3}, same diameter). The size of the plate is the same as that of figure 1, i.e. 40×40 mm^2.

Let us first consider figure 5(*a*), which depicts the velocity u_x above the point $\{x = L/2, y = L/4\}$, on a nodal line. At $t = 0T$, the plate has zero velocity and maximum acceleration. The plate accelerates the gas near the surface and the momentum of the gas is subsequently passed to the higher layers of the fluid. After $t = 0.25T$, the plate decelerates and the gradient of the horizontal velocity in the boundary layer becomes smaller. This sequence repeats itself half a cycle later ($t = 0.5T$), but now in the opposite direction. The grey lines in figure 5(*a*) represent the velocity at two instants during the first half of the cycle ($t = 0.1T$ and $t = 0.4T$) and the black lines at the corresponding instants half a cycle later ($t = 0.6T$ and $t = 0.9T$). Clearly, the velocities during both halves of a cycle cancel each other and the averaged velocity, indicated by the vertical grey line, is zero at this location.

The situation is different half-way between an antinode and a nodal line: figure 5(*b*) shows the velocity above the point $\{x = 3/8L, y = L/4\}$. At this location the plate is not at the same position during the acceleration phase of the first and the second half cycle. As a result, the averaged velocity over one cycle (the grey line with cross markers) does not vanish and a net flow occurs.

Figure 6 shows a vertical cross-section up to $z/H = 0.3$ of the averaged horizontal velocities at $y = L/4$ for $0 < x < L/2$. At the nodal lines ($x = 0, L/2$) and antinodes ($x = L/4$) the averaged velocity is zero. In between, the net velocity is directed towards the nodal lines for $z/H < 0.05$ ($z < 0.100$ mm) and towards the antinodes

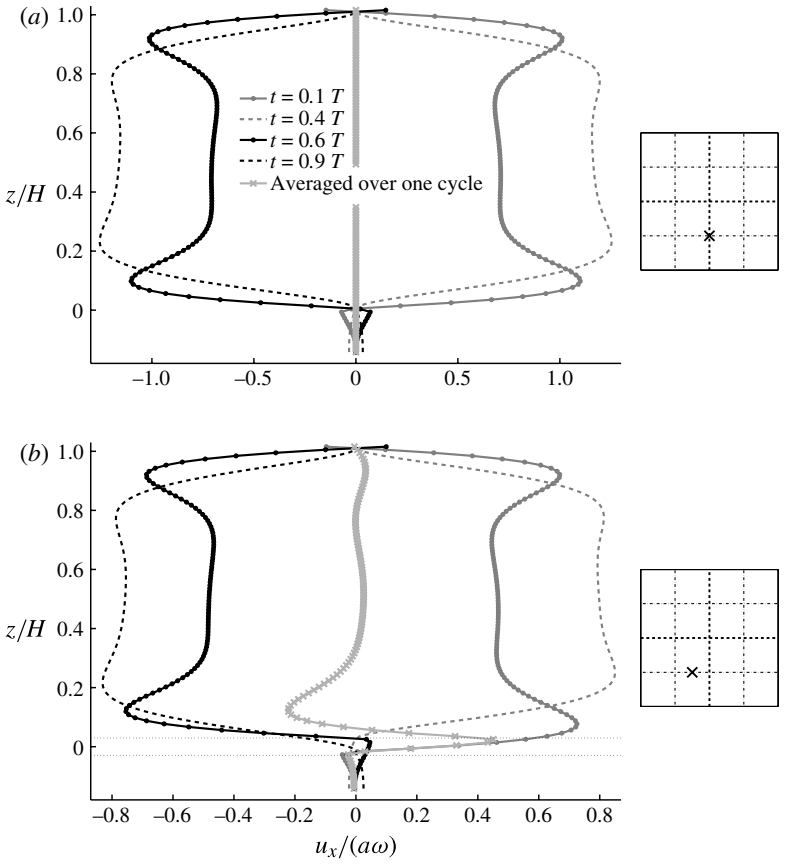

FIGURE 5. Horizontal component u_x of the air velocity induced by the vibrating bottom plate as a function of the height, at two time instants during the first half of a cycle (grey lines) and half a cycle later (black lines). The velocity u_x is given in units of the velocity amplitude $a\omega$ of the vibrating plate; likewise, the height z is normalized by the distance H between the equilibrium position of the vibrating plate and the top lid. The depicted velocities are calculated at two representative locations on the plate (see insets): (*a*) on a nodal line ($x = L/2, y = L/4$) and (*b*) halfway between a nodal line and an antinode ($x = 3/8\,\mathrm{L}, y = L/4$). The grey line with cross markers represents the amplitude of the average velocity during the complete vibration cycle and is multiplied by a factor of five for clarity. At location (*a*) this grey line does not deviate from zero. However, at location (*b*) it deviates from zero, i.e. there is a net flow of air in the horizontal direction.

above this height up to $z/H = 0.30$; see also the grey line with cross markers in figure 5(*b*). Since the particles have a diameter of $d = 0.075$ mm only, based on this result for the streaming flow one would expect the particles to move to the nodal lines. This is in obvious contradiction to the simulation results (see figure 3*b*) where we found that the exact opposite occurs: the particles move to the antinodes.

To resolve this apparent paradox, we now distinguish between the Eulerian and Lagrangian mean velocity of the gas. The Eulerian mean velocity is the net velocity at a point fixed in space. This is the averaged velocity that we have been considering so far (see figure 6 and the grey line with cross markers in figure 5), which would be measured by a probe located at a certain, fixed point in space. In contrast, the

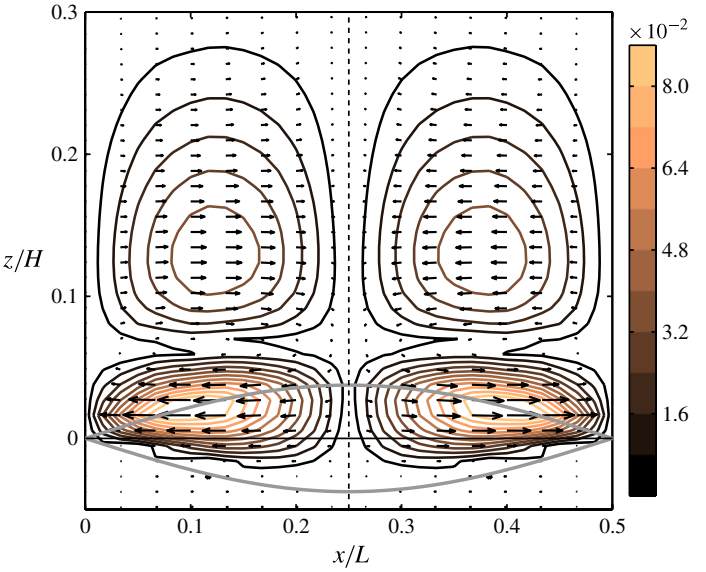

FIGURE 6. (Colour online available at journals.cambridge.org/flm) Cross-section of the time-averaged *Eulerian* velocities in the vertical xz-plane at $y = L/4$. The vertical dashed line marks the position of the antinode at $x = L/4$. The grey lines indicate the location of the plate at maximum deflection. The magnitude of the averaged velocity is indicated by the coloured lines, its direction is indicated by the arrows. The velocity scale has been made dimensionless by dividing by the maximum velocity of the vibrating plate ($a\omega$).

Lagrangian mean velocity is the velocity, again averaged over one cycle, of a tracer particle that moves along with the fluid.

In most studies of steady streaming the Eulerian mean velocity is used (Loh *et al.* 2002; Açikalin, Raman & Garimella 2003; Dorrestijn *et al.* 2007) since the Lagrangian mean velocity is in general much more difficult to obtain analytically. In the present study, however, the Lagrangian mean velocity is definitely the more appropriate: the ratio B for the particles that form inverse Chladni patterns is larger than unity (in our case, $B = 30$) and the Stokesian forces dominate, which means that the particles follow the motion of the fluid and act like tracer particles.

To illustrate the importance of using the Lagrangian mean velocity, we show in figure 7 the trajectories of three tracer particles (or fluid particles) at a height of $d/2 = 0.0375$ mm ($z/H = 0.019$) above the resonating plate (i.e. the same height as the centres of most of the granular particles) during a time span of two vibration cycles. At the antinode the tracer particle moves up and down, while at the nodal line it moves from left to right. In both cases, the tracer particles have the same position after two vibration cycles. In between the antinode and nodal line, however, the tracer particle has moved to the left, i.e. to the antinode. By contrast, the mean Eulerian velocity at this location was directed to the nodal line (see figure 6).

A difference between the time-averaged Eulerian and Lagrangian velocities typically occurs in all oscillatory flows that are inhomogeneous in space and is often referred to as the Stokes drift. This name is a tribute to Stokes' derivation of the expressions that describe the net motion of a small particle near the free surface of water waves (its Lagrangian velocity) in the direction of the wave propagation (Stokes 1847). Lighthill was one of the first to recognize the difference between the Eulerian and

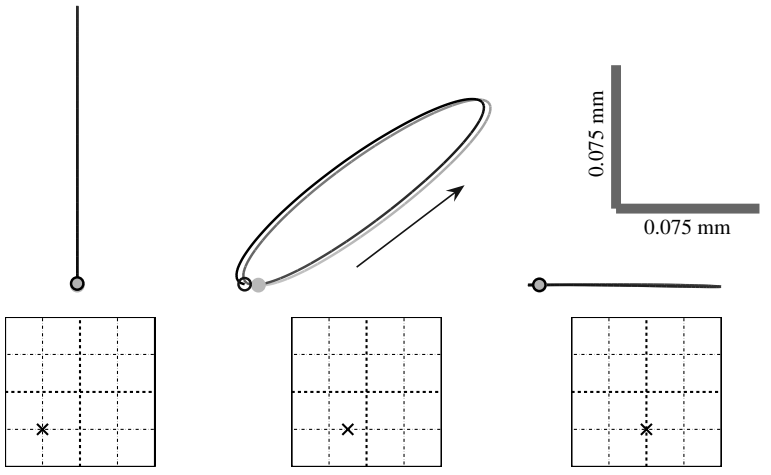

FIGURE 7. Path in the xz-plane of a tracer particle (or fluid particle) during two vibration cycles at an antinode, between an antinode and a nodal line, and at a nodal line, respectively. The initial position of the tracer particles (indicated with the filled grey circles) is 0.0375 mm above the plate, i.e. at the height of the centre of mass of granular particles resting on the plate. The particles at the antinode and the nodal line return exactly to their original position, but the particle between them is seen to move slightly towards the antinode; its position after two cycles is indicated by the black circle. Note that the maximum vertical displacement of the tracer particle at the antinode (left) is twice the vibration amplitude, namely 0.15 mm.

Lagrangian velocities in steady streaming (Lighthill 1978). In that study, however, the streaming was caused by a standing sound wave, and Lighthill correctly reported that the difference between the Eulerian and Lagrangian velocities was considerably smaller than the steady streaming velocity itself. In our case, where the streaming is caused by a resonating plate without significant sound production, the situation is changed dramatically: not only has the difference between the Eulerian and Lagrangian velocities grown significantly, but they are even pointing in opposite directions!

The Lagrangian mean velocity can be determined by subtracting the initial position of a fluid particle (anywhere above the vibrating plate) from its position after one vibration cycle, and dividing by the time T. In figure 8 (the Lagrangian counterpart of figure 6) we have done precisely this, starting the vibration cycle at $t = 0.25T$ when the plate goes through its horizontal equilibrium position. Figure 8(a) shows a vertical cross-section of the Lagrangian streaming velocities at $y = L/4$ for $0 < x < L/2$. Close to the plate (in fact, for all heights $z/H < 0.35$ or $z < 0.7$ mm) the mean velocity is directed towards the antinodes, in stark contrast to the Eulerian velocity depicted in figure 6. Figure 8(b) shows the corresponding horizontal cross section of the time-averaged Lagrangian velocities (above one quarter of the vibrating plate) at a height of half the particle diameter $z = d/2 = 0.0375$ mm ($z/H = 0.019$), which is the height where most particles reside. The inverse Chladni patterns of fine particles are formed as a result of this Lagrangian streaming.

4. Discussion

In the previous Section we have seen that the Lagrangian streaming, which is directed towards the antinodes, is responsible for the inverse Chladni patterns that are observed under experimental conditions similar to the original conditions used

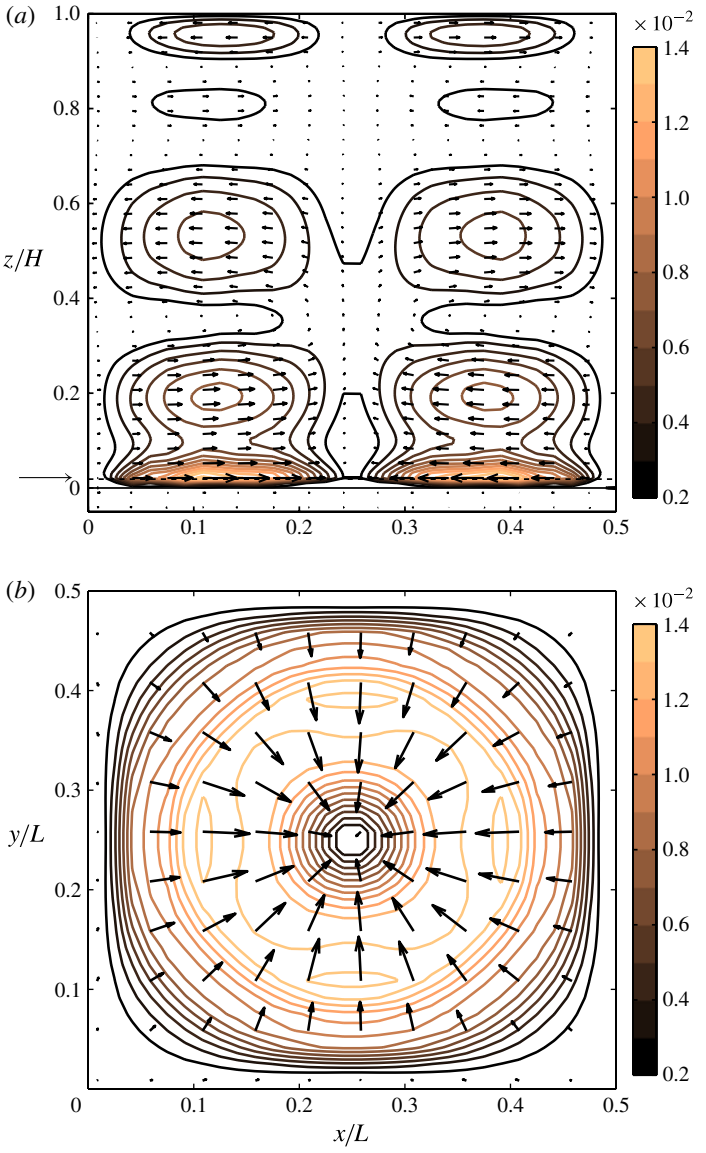

FIGURE 8. (Colour online) (*a*) Cross-section of the time-averaged *Lagrangian* velocities in the xz-plane at $y = L/4$. The magnitude of the averaged velocity is indicated by the coloured lines while the direction is indicated with arrows. Note that the vertical axis goes up all the way to $z/H = 1.0$, whereas the companion cross-section of the Eulerian velocities in figure 6 stops at $z/H = 0.3$. (*b*) Horizontal xy cross-section of the time-averaged Lagrangian velocities of one quarter of the vibrating plate at height $z/H = 0.019$ or $z = d/2 = 0.0375$ mm (indicated by the arrow at the left axis in *a*). In the movie in the online supplementary material one can clearly observe the resulting motion of particles towards their equilibrium positions. Again, the velocity scale has been made dimensionless by dividing by the maximum velocity of the vibrating plate ($a\omega$).

by Chladni and Faraday. At the same time, the Eulerian streaming, the averaged velocity at a fixed position above the plates, has the opposite direction, i.e. towards the nodal lines. At this point one could ask whether, by suppressing the Lagrangian

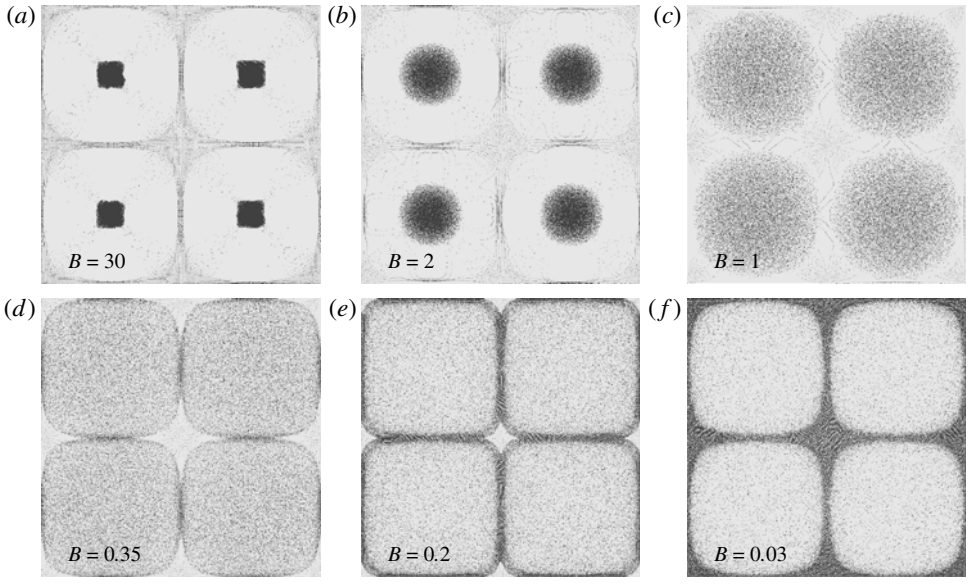

FIGURE 9. Transition from inverse to regular Chladni patterns: 80 000 particles on a resonating plate where the parameter B (equation (2.3)) is varied by modifying the particle density. (*a*) At $B = 30$ the Stokesian forces dominate and an inverse Chladni pattern is formed. (*b–e*) As B decreases, we see a gradual transition towards a regular Chladni pattern. At $B = 1$ ($\rho = 550$ kg m^{-3}) the Newtonian and Stokesian forces balance each other: the particles neither accumulate at the antinodes nor at the nodal lines. (*f*) For $B = 0.03$, the Newtonian forces clearly dominate and a regular Chladni pattern is the result.

component, it would be possible to observe Eulerian streaming in the same system. Stated differently, would it be possible to have air-driven Chladni patterns at the nodal lines? To answer this question let us study the dimensionless parameters that govern the system in some detail.

The first and most important dimensionless parameter is B, the ratio of Stokesian and Newtonian forces on a particle, which was introduced in § 2. In figure 9 we show the complete transition between inverse patterning and regular patterning in our simulation, where we vary B by changing the particle density ρ. When the Stokesian forces dominate ($B > 1$, see (2.3)), the particles are driven to the antinodes (see figure 9*a*). When we slowly increase the density of the particles (with 0.1 % per vibration cycle, allowing the system to adjust itself to the new conditions), the Newtonian forces become more important and the particles start to bounce, forming clouds around the antinodes that become more extended as the density increases (see figure 9*b*). Around $B = 1$ the Newtonian and Stokesian forces are equally strong and the clouds cover almost the entire plate (figure 9*c*). When the density is increased further and B falls below one, the Newtonian forces start to dominate (figure 9*d*,*e*), resulting for $B \ll 1$ in the well-known Chladni pattern with the particles accumulating at the nodal lines (figure 9*f*). Clearly, to observe air-driven (inverse) Chladni patterns, B needs to be considerably larger than one.

The second dimensionless parameter which we can vary is the ratio of the vibration amplitude and the boundary layer thickness, a/δ. We expect that when this parameter is of order unity (or larger), the Lagrangian streaming effect will be dominant. This is the case in our system, as in most Chladni plate experiments. When however the

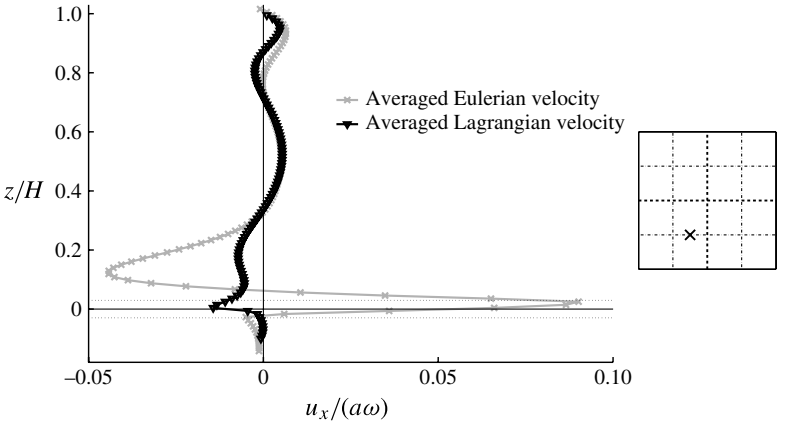

FIGURE 10. Horizontal component u_x of the Lagrangian (black) and Eulerian (grey) streaming velocities as a function of the height above the plate, in the situation of figure 10, i.e. halfway between a nodal line and an antinode ($x = 3/8\,\mathrm{L}$, $y = L/4$, see inset). The velocity u_x is given in units of the velocity amplitude $a\omega$ of the vibrating plate; likewise, the height z is normalized by the distance H between the equilibrium position of the vibrating plate and the top lid. Near the moving plate in the bottom boundary layer, there is a clear difference between the Lagrangian and Eulerian streaming velocities, where they even have opposite directions. By contrast, in the top boundary layer (near the top lid), the Lagrangian and Eulerian streaming velocities are almost equal.

amplitude becomes much smaller than the boundary layer thickness (i.e. $a/\delta \ll 1$), the difference between the Eulerian and Lagrangian streaming becomes vanishingly small. Evidence for this can be found in figure 10, where we compare the Eulerian and Lagrangian streaming velocities as a function of the height above the vibrating plate, for the situation of figure 5(*b*). Close to the plate the Lagrangian streaming is directed towards the antinode, whereas the Eulerian streaming has the opposite direction towards the nodal line. Above the bottom boundary layer this difference vanishes quickly and in the bulk both streaming velocities are practically equal. Incidentally, the same is true for the top boundary layer, which may be interpreted as the Stokes boundary layer in the limit of vanishingly small a/δ ratio. Note that here both streaming velocities are directed towards the nodal lines and particles that are confined to this layer would therefore give rise to a regular Chladni pattern with particles accumulating at the nodal lines.

Sticking to the experimental set-up, i.e. keeping the dimensions and the material of the plate and ambient fluid fixed, we obtain a constant resonant frequency ω for the 2×2 mode and consequently a fixed boundary layer thickness $\delta \approx \sqrt{2\nu/\omega}$. So to go to the domain where the dynamics is dominated by Eulerian streaming, we need to aim for a considerable decrease of the a/δ ratio which can only be realized by decreasing the amplitude a. This has the unfortunate side effect that B (which is proportional to a) will decrease at the same rate through which we enter into the regime that is dominated by the Newtonian forces. Physically this happens because typical air velocities scale as $a\omega$, which leads to a decrease of the drag force on the particles. Therefore, the only option we have to enter the Eulerian streaming regime for the set-up discussed in this article is by at the same time taking much lighter particles, lighter even than lycopodium powder. Alternatively, we may turn the set-up

upside down such that the particles enter the boundary layer near the lid, which indeed produces a Chladni pattern at the nodal lines.

Interestingly, in a recent experiment by Dorrestijn *et al.* (2007) it was found that nanobeads (with a diameter of 0.5 μm) moved towards the nodal lines of a resonating cantilever beam submerged in water, forming a regular Chladni pattern. This result, which at first sight seems to contradict the findings for the classic Chladni experiment, can be interpreted in the light of the above discussion: in their experiment the vibration amplitude ($a \approx 0.02$ μm) is much smaller than the thickness of the boundary layer ($\delta \approx 0.80$ μm), such that $a/\delta \approx 2.5 \times 10^{-2}$, i.e. at least an order of magnitude smaller than it is in the classic experiment of Chladni and Faraday. This is further discussed in appendix B.

Finally, the third parameter is the ratio of the particle diameter and the boundary layer thickness, r/δ. In order to observe the inverse Chladni patterns, particles should be small enough to fit within the boundary layer, such that they can benefit from the difference between the Eulerian and Lagrangian streaming velocities. If the particle radius is of the order of the boundary layer thickness or even larger, particles are expected to move into the outer streaming region. This limit moves beyond the Stokes drag approximation of our analysis, since in this case the incident fluid velocity is not constant but varies considerably over a particle diameter. Also our numerical code would not be suited for this limit, since we would not be able to use the coupling between gas flow and granular dynamics (Stokes, Ergun and Wen-Yu) that is presently being used. Instead, we would have to resolve the air flow around each particle. This clearly requires a numerical approach quite different from the present one.

5. Conclusion

In this paper we have studied the formation of Chladni patterns on a resonating plate by direct numerical simulations, including the flow of the ambient air. We expressly focused our attention on a plate of dimensions similar to the ones originally used in the experiments of Chladni and Faraday.

For heavy particles Newtonian forces dominate ($B \ll 1$) and we find regular Chladni patterns, where particles accumulate around the nodal lines of the resonating plate. For light particles the system is dominated by Stokesian forces ($B \gg 1$), which lead to the formation of inverse Chladni patterns, where particles aggregate at the antinodes. The reason for this behaviour is that the motion of the ambient air averaged over one cycle is non-zero. In particular, the very light particles behave like tracer particles and follow the motion of the air; their motion is appropriately described by the Lagrangian streaming velocity of the air over the resonating plate. Interestingly, Eulerian streaming would give a result that contradicts experiments and simulation, so the streaming phenomenon that causes the inverse Chladni patterns is a striking example of a physical system in which the Lagrangian velocity field proves to be different (and more relevant) than the Eulerian velocity field.

We wish to thank J. A. M. Kuipers for many invaluable discussions on the numerical method, and D. Lohse, H.-J. Stoeckmann and L. van Wijngaarden for carefully reading the manuscript. This work is part of the research program of the Stichting FOM, which is financially supported by NWO.

Supplementary material is available at journals.cambridge.org/flm.

Appendix A. Mathematical description of streaming

In this appendix we give a brief mathematical description of the steady streaming. The basic equation is the momentum balance (i.e. the Navier–Stokes equation) for the gas phase:

$$\frac{\partial(\rho_g \boldsymbol{u})}{\partial t} + \boldsymbol{\nabla}\cdot(\rho_g \boldsymbol{u}\boldsymbol{u}) = -\boldsymbol{\nabla} p - \boldsymbol{\nabla}\cdot\boldsymbol{\tau}, \tag{A 1}$$

where p is the gas phase pressure, ρ_g the density of the gas phase (which we assume to be constant), $\boldsymbol{\tau}$ the viscous stress tensor and $\boldsymbol{u}$ is the flow velocity of the gas phase. One may approximate the velocity and the pressure by a harmonic velocity and pressure (with a zero average over time), plus a time-independent correction representing the steady streaming:

$$\boldsymbol{u} = \boldsymbol{u}^H + \boldsymbol{u}^S, \quad p = p^H + p^S. \tag{A 2}$$

Substituting the harmonic and streaming velocity into (A 1) and averaging over one vibration cycle yields (note that $\langle \boldsymbol{u}\rangle = \boldsymbol{u}^S$, $\langle \boldsymbol{u}^H\rangle = 0$, but $\langle \boldsymbol{u}^H\boldsymbol{u}^H\rangle \neq 0$):

$$\boldsymbol{\nabla}\cdot(\rho_g \boldsymbol{u}^S\boldsymbol{u}^S) = -\boldsymbol{\nabla} p^S - \boldsymbol{\nabla}\cdot\boldsymbol{\tau}^S - \boldsymbol{\nabla}\cdot\langle\rho_g \boldsymbol{u}^H\boldsymbol{u}^H\rangle, \tag{A 3}$$

where the brackets indicate a time averaging over one vibration cycle. As in turbulence modelling, the last term in the equation is commonly called Reynolds stress (Pope 2000). This Reynolds stress drives the steady streaming. For our system, which has negligible compressibility effects, the Reynolds stress in the x-direction at $y = L/4$ is equal to $\rho_g(\partial\langle u_x^2\rangle/\partial x + \partial\langle u_x u_z\rangle/\partial z)$. The second term is large in the boundary layer, where the velocities in both the x- and z-direction are large. For this reason, the steady streaming is much stronger near the vibrating plate than higher up near the cover plate (where the velocity in the z-direction is practically zero), see figures 5(*b*) and 8 in the main text. To obtain an analytical solution for (A 3), one begins by finding a solution for $\boldsymbol{u}^H$ and then substitutes this solution into (A 3) (Nyborg 1953; Açikalin *et al.* 2003). Although in our system the Lagrangian velocity field is more relevant, most studies only consider the Eulerian velocity field (Nyborg 1953; Riley 2001; Açikalin *et al.* 2003; Dorrestijn *et al.* 2007) or the streaming induced by a standing sound wave (Lighthill 1978). Finding the solutions for (A 3) is far from trivial in a three-dimensional system like ours and that is why in this paper we limit ourselves to studying the flow fields obtained from direct simulations.

Appendix B. Chladni patterning when the vibration amplitude is much smaller than the thickness of the boundary layer

As noted in the main text, in the submerged Chladni experiments of Dorrestijn *et al.* (2007) the vibration amplitude a is much smaller than the thickness δ of the boundary layer (table 1). From this it may be inferred that the vertical displacement of the plate can play only a minor role in these experiments. As a result, in this case the difference between the Eulerian and Lagrangian flow fields will only be very small. Indeed, the induced streaming is much more reminiscent of acoustic streaming (Lighthill 1978) and the mechanism responsible for the pattern formation in this case must be quite different from the one discussed in this paper, where $a \sim \delta$. The aim of this appendix is to shed some light on the interpretation of their results in the context of our findings.

In acoustic streaming two layers of vortices can be identified, as depicted in figure 11 (Rayleigh 1884, 1894; Boluriaan & Morris 2003; Hamilton, Ilinskii &

	Present work	Dorrestijn *et al.*
B	10^{-2}–10^{2}	10^{3}–10^{5}
a/δ	0.5	0.01
r/δ	0.5	0.5–5

TABLE 1. Comparison of the three governing dimensionless parameters.

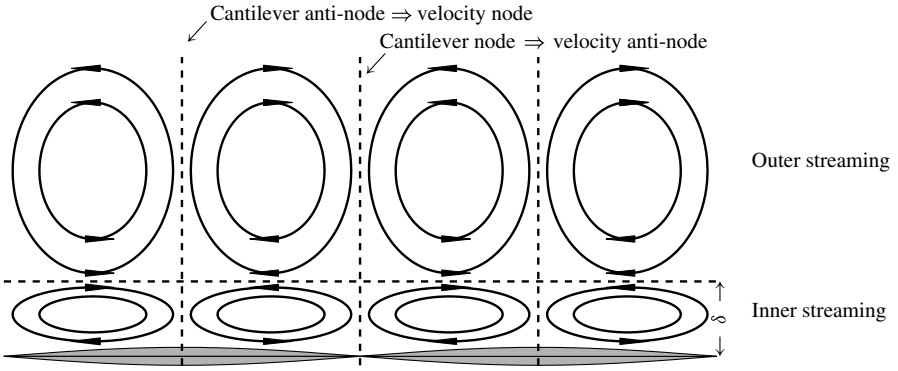

FIGURE 11. Sketch of the proposed streaming pattern in the experiment conducted by Dorrestijn *et al.* (2007), with particles on a cantilever beam submerged in water, resonating at very high frequency with a very small amplitude a. The vertical vibration of the beam induces a velocity field in the fluid: the horizontal component of this field is zero at the beam's antinodes and maximal at the nodes (cf. figure 2). In other words, the velocity nodes are located at the antinodes of the resonating beam and vice versa.

Zabolotskaya 2003): vortices inside the boundary layer (inner circulation) and vortices outside the boundary layer (outer circulation), which have an opposite direction of rotation. Particles smaller than the thickness of the boundary layer will be dragged by the inner circulation to the nodal lines; particles with a diameter exceeding 2δ (such that their centre of mass lies above the boundary layer) are exposed to the outer circulation and will go to the antinodes. In the experiment of Dorrestijn *et al.* (2007) the thickness of the boundary layer was $\delta \approx \sqrt{2\nu/\omega} = 0.8$ μm, where $\nu = 1.00 \times 10^{-6}$ m^2 s^{-1} is the kinematic viscosity of water and $\omega = 2\pi f = 3,14 \times 10^6$ s^{-1} (with $f = 0.5$ MHz the frequency of the vibrating plate). In perfect agreement with the mechanism outlined above they found that nanobeads with a diameter of 0.5 μm, i.e. smaller than δ, moved to the nodal lines, and large particles towards the antinodes.

Incidentally, according to the authors' own analysis (Dorrestijn *et al.* 2007) the inner circulation responsible for the motion of the nanobeads was confined to the layer of vibration just as in figure 5 of Açikalin *et al.* (2003). However, in the experiment this layer had a thickness of only $a \approx 0.02$ μm, much too small to drive the 0.5 μm nanobeads. If our interpretation in terms of acoustic streaming is correct, the actual situation is as depicted in figure 11 and the zone of inner circulation is given by the thickness of the boundary layer $\delta = 0.8$ μm.

REFERENCES

AÇIKALIN, T., RAMAN, A. & GARIMELLA, S. V. 2003 Two-dimensional streaming flows induced by resonating, thin beams. *J. Acoust. Soc. Am.* **114**, 1785.

BANERJEE, S. & LAW, S. E. 1998 Characterization of chargeability of biological particulates by triboelectrification. *IEEE Trans. Indust. Appl.* **34**, 1201.

BEETSTRA, R., VAN DER HOEF, M. A. & KUIPERS, J. A. M. 2007 Drag force of intermediate Reynolds number flow past mono- and bidisperse arrays of spheres. *AIChE J.* **53**, 489.

BOLURIAAN, S. & MORRIS, P. J. 2003 Acoustic streaming: from Rayleigh to today. *Intl J. Aeroacoust.* **2**, 255.

BRENNER, H. 1961 The slow motion of a sphere through a viscous fluid towards a plane surface. *Chem. Engng Sci.* **16**, 242.

CHLADNI, E. F. F. 1802 *Die Akustik*. Breitkopf & Härtel.

CHLADNI, E. F. F. 1809 *Traité d'Acoustique*. Courcier.

DEEN, N. G., VAN SINT-ANNALAND, M. & KUIPERS, J. A. M. 2004 Multi-scale modelling of dispersed gas–liquid two-phase flows. *Chem. Engng Sci.* **59**, 1853.

DORRESTIJN, M., BIETSCH, A., AÇIKALIN, T., RAMAN, A., HEGNERAND, M., MEYER, E. & GERBER, CH. 2007 Chladni figures revisited based on nanomechanics. *Phys. Rev. Lett.* **98**, 026102.

ELGHOBASHI, S. 1994 On predicting particle-laden turbulent flows. *Appl. Sci. Res.* **52**, 309.

ERGUN, S. 1954 Fluid flow through packed columns. *Chem. Engng Prog.* **48**, 89.

FARADAY, M. 1831 On a peculiar class of acoustical figures; and on certain forms assumed by groups of particles upon vibrating elastic surfaces. *Phil. Trans. R. Soc. Lond.* **121**, 299.

VAN GERNER, H. J. 2009 Newton versus Stokes: competing forces in granular matter. PhD thesis, Enschede, http://purl.org/utwente/61070.

GOLDMAN, A. J., COX, R. G. & BRENNER, H. 1967 Slow viscous motion of a sphere parallel to a plane wall – I Motion through a quiescent fluid. *Chem. Engng Sci.* **22**, 637.

HAMILTON, M. F., ILINSKII, Y. A. & ZABOLOTSKAYA, E. A. 2003 Acoustic streaming generated by standing waves in two-dimensional channels of arbitrary width. *J. Acoust. Soc. Am.* **113**, 153.

VAN DER HOEF, M. A., YE, M., VAN SINT ANNALAND, M., ANDREWS IV, A. T., SUNDARESAN, S. & KUIPERS, J. A. M. 2006 Multi-scale modelling of gas-fluidized beds. *Adv. Chem. Engng* **31**, 65.

VAN DER HOEF, M. A., VAN SINT ANNALAND, M., DEEN, N. G. & KUIPERS, J. A. M. 2008 Numerical simulation of dense gas–solid fluidized beds: a multiscale modelling strategy. *Ann. Rev. Fluid Mech.* **40**, 47.

LIGHTHILL, J. 1978 Acoustic streaming. *J. Sound Vib.* **61**, 391.

LOH, B.-G., HYUN, S., RO, P. I. & KLEINSTREUER, C. 2002 Acoustic streaming induced by ultrasonic flexural vibrations and associated enhancement of convective heat transfer. *J. Acoust. Soc. Am.* **111**, 875.

MAXEY, M. & RILEY, J. 1983 Equation of motion for a small rigid sphere in a non-uniform flow. *Phys. Fluids* **26**, 883.

NYBORG, W. L. 1953 Acoustic streaming due to attenuated plane waves. *J. Acoust. Soc. Am.* **25**, 68.

PESKIN, C. S. 2002 The immersed boundary method. *Acta Numerica* **11**, 480.

POPE, S. B. 2000 *Turbulent Flows*. Cambridge University Press.

RAYLEIGH, L. 1884 On the circulation of air observed in Kundt's tubes, and on some allied acoustical problems. *Phil. Trans. R. Soc. Lond.* **125**, 1.

RAYLEIGH, L. 1894 *The Theory of Sound,* vol. I. Macmillan.

RILEY, N. 2001 Steady streaming. *Annu. Rev. Fluid Mech.* **33**, 43.

SAVAGE, S. B. 1988 Streaming motions in a bed of vibrationally fluidized dry granular material. *J. Fluid Mech.* **194**, 457.

STÖCKMANN, H.-J. 2006 Ein Nomade der Wissenschaft. *Physik J.* **5**, 47.

STÖCKMANN, H.-J. 2007 Chladni meets Napoleon. *Eur. Phys. J. Special Topics* **145**, 15.

STOKES, G. G. 1847 On the theory of oscillatory waves. *Camb. Phil. Soc. Trans.* **8**, 441.

UHLMANN, M. 2005 An immersed boundary method with direct forcing for the simulation of particulate flows. *J. Comput. Phys.* **209**, 448.

WALLER, M. D. 1955 Air circulations about a vibrating plate. *Br. J. Appl. Phys.* **6**, 347.